

UKAEA-CCFE-PR(20)110

D. Hoare, F. Militello, J.T. Omotani, F. Riva, S.
Newton, T. Nicholas, D. Ryan, N.R. Walkden

Dynamics of Scrape-Off Layer Filaments in high beta plasmas

Enquiries about copyright and reproduction should in the first instance be addressed to the UKAEA Publications Officer, Culham Science Centre, Building K1/O/83 Abingdon, Oxfordshire, OX14 3DB, UK. The United Kingdom Atomic Energy Authority is the copyright holder.

The contents of this document and all other UKAEA Preprints, Reports and Conference Papers are available to view online free at scientific-publications.ukaea.uk/

Dynamics of Scrape-Off Layer Filaments in high beta plasmas

D. Hoare, F. Militello, J.T. Omotani, F. Riva, S. Newton, T. Nicholas, D. Ryan, N.R. Walkden

Dynamics of Scrape-Off Layer Filaments in high β plasmas

D. Hoare^{1,2}, F. Militello¹, J.T. Omotani¹, F. Riva¹, S. Newton¹,
T. Nicholas^{1,3}, D. Ryan¹ and N.R. Walkden¹

¹ Culham Centre for Fusion Energy, Abingdon, Oxon, OX14 3EB

² Department of Physics, University of Bath, Bath, BA2 7AY

³ Department of Physics, University of York, Heslington, York YO10 5DD, UK

Abstract. The role of magnetic perturbations generated by filaments in the scrape-off layer is investigated by performing simulations of 3D seeded filaments with an electromagnetic numerical code which includes sheath boundary conditions. Depending on the plasma β , three smoothly connecting regimes were identified: an electrostatic regime where the magnetic field is substantially unaffected by the motion of the filament, an intermediate regime where the magnetic field is excited but relaxes within the filament's lifetime and an electromagnetic regime where the frozen-in condition is well satisfied. The electromagnetic effects are found to have a significant impact on the filament dynamics at values of β relevant for fusion devices, including increased midplane radial velocity, bending of the filament and braiding of magnetic field lines. Importantly, a finite Alfvén speed can allow electrical disconnection of the target and the upstream part of the filament, thus removing the slowing down effect associated with the sheath and producing faster filaments and more intense cross-field transport in perturbations that were affected by the sheath in the $\beta = 0$ limit.

1. Introduction

Filaments, also known as blobs, are field aligned coherent plasma perturbations that form in the boundary region of magnetic fusion devices and pass into the Scrape-Off Layer (SOL) [1]. Depending on the plasma regime, filaments can impart large quantities of particles and energy onto the first wall, making control, and therefore understanding, of these structures a priority to prepare for larger reactor relevant tokamaks of the future.

Diagnostics, such as fast cameras that capture microsecond time scales [2, 4, 3, 5], Langmuir probes [6, 7, 8, 9, 10, 11, 12] and gas puff imaging [13, 14, 15, 16, 17] provide a wealth of data useful to characterise the filaments but several aspects behind their global dynamics still need to be clarified. Numerical simulations can help in developing a more sophisticated understanding, with the experimental observations as a basis to estimate filament properties for use in seeded filament simulations. These allow for the dynamics of isolated individual filaments to be studied and to validate physics models by comparing the model evolution to experimental data [20, 5]. Several 2D and 3D fluid codes exist that can perform these simulations such as STORM [21, 22, 23, 5], GBS [27, 28], HESEL [29, 30] and TOKAM3X [31], which use similar but distinct models and numerical approaches.

Filaments have been extensively studied in electrostatic regimes where the magnetic field does not evolve with time, however little work exists studying the electromagnetic regime [33, 34, 35, 36, 38, 39, 40]. This regime might be relevant to large L-mode filaments, inter-ELM filaments and, most likely, ELMs. The importance of the electromagnetic

effects is typically characterised by the parameter $\beta = 2\mu_0 p/B^2$, which represents the ratio between the kinetic plasma pressure, p , and the magnetic plasma pressure, $B^2/(2\mu_0)$. The electrostatic limit assumes β and the terms associated with it in the model to be negligibly small, while the electromagnetic effects become relevant in plasmas where β achieves rather small but finite values often calculated using linear physics arguments (see e.g. [41] for a comprehensive review). In particular, for the problem we will be tackling (fluid limit, simplified geometry without magnetic shear) these arguments suggest that the electrons have an electromagnetic parallel response when β is comparable to or larger than the mass ratio m_e/m_i and the corresponding linear eigenmodes have a significant electromagnetic component when β is of the order of $(L_\perp/L_\parallel)^2$, where L_\perp and L_\parallel are typical perpendicular and parallel length scales of the system. Estimating a nonlinear criterion for electromagnetic behaviour is less trivial [41]. A possible formulation of such a criterion for filament physics will be presented in this paper.

The motion of filaments is governed by $\mathbf{E} \times \mathbf{B}$ drifts, where electric fields result from the interaction between pressure gradients and magnetic curvature effects [47, 1]. The electric fields involved are driven by the currents flowing in the filament which can take paths parallel (parallel current, \mathbf{J}_\parallel) or perpendicular (diamagnetic, \mathbf{J}_d , or polarisation, \mathbf{J}_p , currents) to the confining magnetic field. In general, the relative strengths of these currents, and therefore the dominant balance in the charge conservation equation, depend on properties of the filament such as its perpendicular size [47, 48, 24], resistivity [48, 22] or magnetic shear of the equilibrium [48]. In the electromagnetic treatment, the currents generate perturbed magnetic fields. Naturally, larger currents are driven when the pressure perturbation associated with the filament is larger.

Another interesting observation is that filaments crossing the separatrix experience a change in the topology of the equilibrium magnetic field. In the presence of non-negligible electromagnetic effects reconnection processes might be involved, possibly affecting particle and heat exhaust in the proximity of the last closed flux surface all the way down to the strike point (i.e. the region where the separatrix hits the target) a subject that will be discussed in a follow up paper [49]. The underlying electromagnetic physics presented in this paper provides solid basis for future, more complex investigations.

Some properties of filament dynamics in electromagnetic regimes were already investigated in literature. D'Ippolito *et al.* [45] and Krasheninnikov *et al.* [37] introduced a first basic theoretical interpretation that is closely related with the ballooning criterion $\alpha_{MHD} = \beta L_\parallel^2 / (RL_\perp) \gg 1$, which comes from balancing the ballooning growth rate with the inverse of the parallel Alfvén time, representing the field line bending stabilisation. Ribeiro and Scott [33, 36] analysed gyrofluid electromagnetic simulations in the plasma edge, both on open and closed field lines, but their emphasis was on turbulence, not on the electromagnetic features associated with filaments. Xu *et al.* [38] introduced the concept of a filament as a drift Alfvén vortex, of coupling with shear Alfvén waves and field line bending associated with the pressure perturbation. Finally, Lee *et al.* [39, 40] demonstrated with 3D numerical simulations that field line bending occurs and that a finite Alfvén speed can lead to faster radial propagation. Also, they showed that drift wave instabilities within the filament can be stabilized by electromagnetic effects, thus leading to a more coherent structure.

In our contribution, we extend the work done in Refs. [39, 40] by providing a quantitative description of the electromagnetic effects on filament dynamics and by introducing a non-linear criterion to assess the level of the electromagnetic effects. Our results are obtained with 3D drift fluid simulations carried out with a newly extended version of the STORM module [21] of the BOUT++ code [26]. In particular, we study the β dependence of the radial velocity and identify when the transition between electrostatic and electromagnetic regimes occurs. Finally, we will devote particular attention to the dynamics of the magnetic field lines perturbed by the passage of the filament, which

respond in qualitatively different ways depending on the local β of the filament and can be entrained within it for a significant amount of time, thus satisfying the frozen in condition on the time scale considered.

2. Model

A simplified slab geometry is used, with target plates normal to the magnetic field lines. The magnetic field and the radial direction comprise two of the orthogonal directions, z and x respectively, with the third, y , normal to both, named binormal. The background magnetic field, $\mathbf{B}_0 = B_0 \hat{\mathbf{z}}$, with $\hat{\mathbf{z}}$ the unit vector along z , is considered to be constant in direction and amplitude. The numerical domain is chosen to represent MAST scales [12, 5]. The filaments are evolved between two identical targets at opposite ends of the numerical domain at $z = \pm L_z$, and the model can be run inside the full domain or with a symmetry condition imposed at the midplane (assuming up-down symmetry as in a double null configuration). The midplane is defined as the plane parallel to and half way between the two targets. Unless stated otherwise, in our simulations, we used an $[x, y, z]$ grid of $128 \times 128 \times 32$ points with $L_x = L_y = 100$ and $L_z = 2692.3$ in normalized units (defined later), corresponding to $L_x = L_y \approx 13\text{cm}$ and $L_z \approx 345\text{cm}$. Some of the simulations presented in the following were repeated with L_z twice as large to describe conditions more relevant for MAST (but at a larger computational cost since we also double the number of parallel grid points to maintain constant resolution).

The equations used in this work are an extension of previous versions of the STORM model, the full details of which are presented elsewhere [21, 23, 24, 5]. They represent a finite β , drift ordered, anisotropic fluid model with cold ions and arbitrary fluctuation amplitude (i.e. the Boussinesq approximation is not used). The closure is collisional, allowing for neoclassical transport in the SOL [25]. The updates to the model presented in this paper are centred on the relaxing of the electrostatic approximation.

The equations solved here are given in normalised form as:

$$\frac{\partial \varpi}{\partial t} + [\phi, \varpi] = -U \nabla_{\parallel} \varpi - [v_{E \times B}^2 / 2, n] - \frac{\hat{g}}{n} \frac{\partial n}{\partial y} + \frac{1}{n} \nabla_{\parallel} J_{\parallel} + \mu_v \nabla_{\perp}^2 \varpi \quad (1)$$

$$\frac{\partial n}{\partial t} + [\phi, n] = -\nabla_{\parallel} (nV) + n \hat{g} \frac{\partial \varphi}{\partial y} - \hat{g} \frac{\partial (nT)}{\partial y} + D \nabla_{\perp}^2 n + S_n \quad (2)$$

$$\frac{\partial \mathcal{X}_U}{\partial t} + [\phi, U] = -U \nabla_{\parallel} U - \nabla_{\parallel} \varphi - \frac{\eta_{\parallel}}{\mu} J_{\parallel} + 0.71 \nabla_{\parallel} T - \frac{S_n U}{n} \quad (3)$$

$$\frac{\partial \mathcal{X}_V}{\partial t} + [\phi, V] = -V \nabla_{\parallel} V + \mu \left(\nabla_{\parallel} \varphi - \frac{1}{n} \nabla_{\parallel} (nT) + \eta_{\parallel} J_{\parallel} - 0.71 \nabla_{\parallel} T \right) - \frac{S_n V}{n} \quad (4)$$

$$\begin{aligned} \frac{\partial T}{\partial t} + [\phi, T] &= -V \nabla_{\parallel} T \\ &+ \frac{2}{3n} (0.71n(U - V) \nabla_{\parallel} T - \nabla_{\parallel} q_{\parallel} - nT \nabla_{\parallel} V - \eta_{\parallel} n^2 (U - V)^2) \\ &+ \frac{2\hat{g}}{3n} \left(T^2 \frac{\partial n}{\partial y} - nT \frac{\partial \varphi}{\partial y} + \frac{7}{2} nT \frac{\partial T}{\partial y} + \frac{1}{\mu} V^2 \frac{\partial nT}{\partial y} \right) \\ &+ \frac{2}{3n} S_E + \frac{S_n V^2}{3\mu n} - \frac{TS_n}{n} + \frac{2}{3n} \kappa_{\perp} \nabla_{\perp}^2 T, \end{aligned} \quad (5)$$

where ϖ is the generalised vorticity (the Boussinesq approximation is *not* made), n is the plasma density, \mathcal{X}_U and \mathcal{X}_V are combinations of respectively ion and electron velocities, U and V , with the parallel component of the vector potential ψ , T is the electron temperature, φ is the electrostatic potential, \hat{g} is the artificial gravity term to account for the magnetic field curvature, D is the collisional particle diffusivity coefficient, S_n and S_E are particle and energy sources (defined below), η_{\parallel} is resistivity, μ_v is the ion viscosity, κ_{\perp} is the

perpendicular thermal diffusivity coefficient and $\mu = m_i/m_e$ is the mass ratio. Also, $v_{E \times B} = |\hat{\mathbf{z}} \times \nabla \phi|$ is the modulus of the $\mathbf{E} \times \mathbf{B}$ velocity and the Poisson bracket is defined as: $[f, g] = (\hat{\mathbf{z}} \times \nabla f) \cdot \nabla g$, where f and g are generic functions. The conductive heat flux, q_{\parallel} is given by:

$$q_{\parallel} = -\kappa_{\parallel,0} T^{5/2} \nabla_{\parallel} T - 0.71 n T (U - V), \quad (6)$$

with $\kappa_{\parallel,0}$ is the temperature independent part of the thermal conductivity. These equations are closed by:

$$\varpi = \nabla \cdot (n \nabla_{\perp} \varphi), \quad (7)$$

$$J_{\parallel} = -\nabla^2 \psi, \quad (8)$$

with the parallel current, $J_{\parallel} = n(U - V)$, and the electromagnetic velocities:

$$\mathcal{X}_U = U + \frac{\beta}{2} \psi, \quad (9)$$

$$\mathcal{X}_V = V - \mu \frac{\beta}{2} \psi. \quad (10)$$

The normalisation used in the model is the Bohm normalisation, details can be found in [5]. Time scales are normalised by the ion gyro-frequency, $\Omega_i = eB/m_i$ and length scales by the hybrid gyro-radius, $\rho_s = c_s/\Omega_i$, where $c_s = \sqrt{T/m_i}$ is the sound speed, m_i is the ion mass and e is the electron charge. The electrostatic potential, ϕ is normalised by T/e and the plasma density, n , is normalised to a background density. The electromagnetic potential is normalised by $\psi \rightarrow \frac{\beta}{2} \frac{m_i c_s}{e} \psi$. Our reference values for the normalisation are: electron temperature $T_{e,0} = 20eV$, plasma density $n_0 = 0.5 \times 10^{19} m^{-3}$, safety factor $q_{95} = 7$, magnetic field $B_0 = 0.5T$ and curvature radius $R_c = 1.5m$. These are typical MAST values used also in previous publications, see e.g. [42]. Using the expressions in [21] we find that these values give: $\mu_v = 5.85 \times 10^{-2}$, $D = 2.98 \times 10^{-3}$, $\eta_{\parallel} = 4.28 \times 10^{-2}$, $\kappa_{\parallel,0} = 1.37 \times 10^5$, $\kappa_{\perp} = 8.52 \times 10^{-3}$ and $\hat{g} = 1.71 \times 10^{-3}$. Finally, using deuterium, $\mu = 3.64 \times 10^3$.

The background plasma upon which the filament evolves is produced by imposing the following sources of particles and energy:

$$S_n(z) = C_1 \frac{10e^{\frac{10z}{L_z}}}{L_z(e^{10} - 1)}, \quad (11)$$

$$S_E(z) = C_2 \frac{e^{-\frac{5z}{L_z}}}{L_z}, \quad (12)$$

where C_1 and C_2 were adjusted until the midplane value (at $z = 0$) of the normalised density and temperature reached 1. In our simulations, this was obtained for $C_1 = 0.595$ and $C_2 = 14.25$.

Initial conditions for filament seeding are discussed in detail in previous papers, see e.g. [5]. In this paper, filaments were seeded as density perturbations with the temperature of the background plasma, since parallel heat transport is very efficient and it smooths temperature perturbations quite rapidly. A radially symmetric Gaussian profile, with width $w = 5\rho_s \approx 6mm$, was used in the perpendicular direction and a profile in the parallel direction, given by:

$$\rho(z) = \frac{1}{2} A \left[1 - \tanh \left(\frac{z - L_f}{\delta_z} \right) \right], \quad (13)$$

where A is the amplitude of the density perturbation with respect to background and z goes from 0 at the midplane to L_z at the target. We took $\delta_z = 0.1L_z$ and $L_f = L_z$ for simulations analysing the dynamics of the filament, whilst $L_f = 0.5L_z$ for those focusing on the field line behaviour. The former choice represent an almost completely homogeneous perturbation, while the latter a filament that is localized above the X-point.

2.1. Electromagnetic Terms in the Model

In this Section, we briefly discuss how finite β effects enter our physical model. In the electrostatic regime, the inductive part of the electric field \mathbf{E} is neglected. In the finite β drift ordering, appropriate for the filament dynamics, we have [50]:

$$\begin{aligned}\mathbf{E}_\perp &= -\nabla_\perp\varphi, \\ \mathbf{E}_\parallel &= -\nabla_\parallel\varphi - \frac{\beta}{2}\frac{\partial\psi}{\partial t}\hat{\mathbf{z}},\end{aligned}\tag{14}$$

where the perpendicular component remains electrostatic to leading order [50], while the parallel field becomes electromagnetic. This relates to the magnetic field, \mathbf{B} , which is a combination of the static background field, $B_0\hat{\mathbf{z}}$, and the perturbed, time varying field induced by the filament:

$$\mathbf{B} = B_0\hat{\mathbf{z}} + \frac{\beta}{2}\nabla \times (\psi\hat{\mathbf{z}}).\tag{15}$$

The correction applied in this way gives a magnetic field that has a perturbed direction but approximately the same magnitude, taken to be B_0 . Therefore, the definition of the parallel gradient operator has to be updated to include the second term on the right-hand side:

$$\nabla_\parallel = \nabla_{\parallel 0} + \frac{\beta}{2}[\nabla \times (\psi\hat{\mathbf{z}})] \cdot \nabla,\tag{16}$$

where $\nabla_{\parallel 0} = \hat{\mathbf{z}} \cdot \nabla$ was the electrostatic operator.

2.2. Boundary Conditions

On the time scales involved in filament dynamics, the materials surrounding the plasma can be treated as perfect conductors as their magnetic response is slow. In a perfect conductor, the magnetic field is frozen and no perturbation can arise. We are therefore led to assume that $\nabla \times (\psi\hat{\mathbf{z}}) = 0$ and so $\psi = 0$. This is known as the 'line tying' boundary condition in literature.

While this would be a correct assumption in solar physics, where a hotter plasma background would represent the ideal conductor, it fails when the plasma is in contact with a material surface, such as the divertor targets. This is because at the interface, a Debye sheath is formed, the entrance of which is the typical boundary of the fluid simulations. In this case, taking $\psi = 0$ is inconsistent for perpendicular targets as it would lead, through 8, to the conclusion that no parallel current can enter the domain boundaries, which is incorrect in the presence of perturbations. Given these considerations, ψ at the target (i.e. at $z = \pm L_z$) should be obtained by inverting 8 for the current J_\parallel given by Bohm's boundary condition.

Despite the fundamental conceptual difference between the two approaches, numerical simulations we performed showed that the effect on the dynamics of the filaments was negligible. As a consequence, most of the results presented here are obtained with the standard line tying condition, which is numerically less expensive. It is likely that the time scale of the simulation duration allows for this approximation, with longer dynamics requiring a more rigorous approach.

Perpendicular and parallel boundary conditions on other fields are identical to those used in previous STORM publications, see e.g. [21, 23, 5]

3. Results

Filaments are seeded onto the equilibrium background plasma, generated as discussed above, and evolved for approximately 20-30 μs , the time scale typical of experimental filaments [5]. The parameter β is varied to isolate electromagnetic effects without

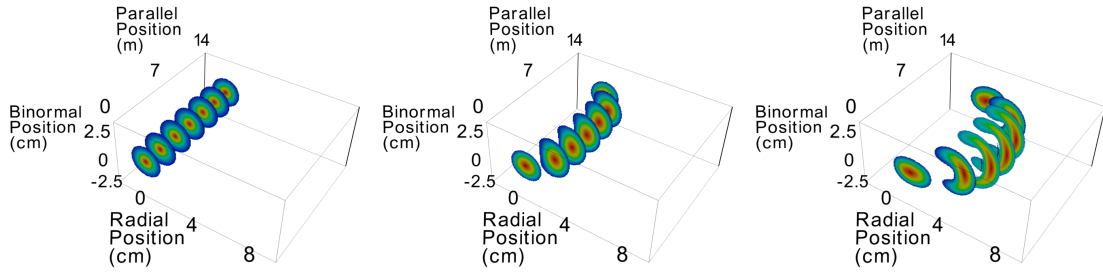


Figure 1. Density contours of a filament from target to target in the parallel direction at the start of the simulation and after $10\mu\text{s}$ and $20\mu\text{s}$. Contours are shown as drift plane slices, with normalised densities between 0.2 (blue) and 8 (red) above the background density.

changing the filament pressure or background magnetic field, density or temperature. All other dimensionless parameters are kept at their original value. While this is clearly not representative of actual experimental scans, which typically vary all dimensionless parameters, this reductionist approach is used here to isolate and emphasise the β dependence of the overall dynamics. Note that at the nominal normalising parameters, $\beta \approx 1.6 \times 10^{-4}$ but this underestimates the effective β in MAST as the magnetic field on the low field side is typically lower than this (around $0.1 \div 0.2$ T rather than 0.5 used here and in previous STORM publications). Other investigations have discussed amplitude, density and temperature effects on filament dynamics (see e.g. [43] for a comprehensive analysis), which we expect to interact with those discussed here.

A typical example of the evolution of a high β filament in the electromagnetic regime is shown in figure 1. In this case, $\beta = 1.6 \times 10^{-2}$ and the peak filament density amplitude was 8 times the background density (i.e. $A = 8$). These parameters represent an extreme simulation, with a combination of high filament amplitude and plasma β , unlikely to occur experimentally. However, these extreme values showcase the qualitative electromagnetic effects at work in realistic filaments in fusion devices, which can have the same β at typically lower amplitude.

A key behaviour of electromagnetic filaments observed in previous studies [39, 40] is filament bending, where the centre of the filament bulges forwards of the ends of the filaments. As seen in Fig.1, this behaviour is replicated within the STORM model as β is increased. This can be understood as a combination of the perturbation of the magnetic field direction, but also due to an increased localisation of dynamics coupled with the density profile of the filament. Filament bending will be explored in more depth in relation to electromagnetic field propagation.

3.1. Radial Velocities and Scaling

As filament studies seek to understand the cross-field particle transport in the SOL, the filament radial velocity is important. Combined with the filament density, the velocity affects the rate of particle transfer and thus the SOL profile. The radial velocity is calculated by defining the location of the filament by its centre of mass in each drift plane (i.e. $x - y$ plane, where the drifts take place), calculated with a small threshold to ignore the background plasma. In this work a threshold of 20% above nominal background level is used. We start by investigating the effect of β and of the density amplitude, A , on the maximal radial velocity. This velocity is measured at both the midplane and near the target in order to capture information about the parallel bending of the filament.

The results of varying plasma β and the filament amplitude are shown in Fig. 2. Each β corresponds to a given Alfvén velocity, $v_A = \sqrt{\frac{2}{\beta}}c_s$, which represents the typical velocity

of the waves which propagate the electromagnetic potentials in the parallel direction, which in turn drive the filament's perpendicular motion through the $\mathbf{E} \times \mathbf{B}$ drift.

It is useful to briefly elaborate on this important concept. In a finite β drift model such as ours, kinetic drift Alfvén waves [41] can be excited by pressure perturbations, such as those associated with a filament. These waves can communicate variations in the electrostatic potential, ϕ , throughout the system. When a filament enters the SOL, it excites waves that travel towards the target and reflect back, communicating to the upstream plasma the presence of the sheath. The latter would tend to slow down the motion of sufficiently wide filaments (above a critical width [44]) by acting as a current drain and thus weakening the convective cells associated with the filament potential (remember that ϕ is the stream function for the $\mathbf{E} \times \mathbf{B}$ velocity). This happens very rapidly in the electrostatic regime (at infinite speed if there is no electron inertia), but at finite β the travelling waves take a finite time $\Delta t = 2L_{\parallel}/v_A \propto L_{\parallel}\sqrt{\beta}$ to do the round trip. If in this time the filament has moved more than its width across the field, the information associated with the presence of the target will not reach it and therefore the filament perturbation will move as if the sheath did not exist.

It can be expected that electromagnetic effects become important when the Alfvén waves can no longer propagate fast enough to keep the upstream and downstream region of the filament in communication. This interpretation can be applied to usefully define a nonlinear electromagnetic condition for filaments. Taking L_{\perp} as the typical length scale associated with the electrostatic potential structure of the filament, and V_{\perp} the typical radial filament velocity at the parallel midpoint, the electrostatic regime is valid only if $\Delta t \ll L_{\perp}/V_{\perp}$ or equivalently, $\sqrt{\beta} \frac{L_{\parallel}}{L_{\perp}} \ll \frac{c_s}{V_{\perp}}$. A similar interpretation was introduced in [45], where the discussion was limited to ideal MHD instabilities. To see electromagnetic effects in a 14 meter target to target filament ($2L_{\parallel}$) as in the MAST experiment, with a characteristic peak velocity of 1 km/s (V_{\perp}) and a 1 cm width (L_{\perp}), the Alfvén speed must be slower than approximately 1400 km/s (v_A), corresponding to a plasma β larger than around 1×10^{-3} if $c_s \approx 30$ km/s, which is typical for MAST [5]. All these points are compatible with the results shown in the right panel of Fig.2 (which uses realistic L_{\parallel}).

At small β (high v_A), the radial velocities of the filaments are identical at the target and midplane. This coincides with the electrostatic regime, $\beta \ll (L_{\perp}c_s)^2/(L_{\parallel}V_{\perp})^2$, where the potential is communicated instantaneously along the parallel direction and so the filament travels coherently. As the β value increases (v_A decreases), the electromagnetic regime, $\beta \gg (L_{\perp}c_s)^2/(L_{\parallel}V_{\perp})^2$, is entered where the midplane velocity increases beyond the target velocity. The discrepancy between these two values for a filament is indicative of the filament bending. The target velocity tends towards zero due to line tying at the boundary and increasing freezing of the field lines in the plasma, as in ideal MHD. The field line can not move at the boundary, and the plasma can slip less and less efficiently as β grows. Note that, as predicted by our non-linear criterion for this specific case, the radial propagation velocity starts to be affected when $\beta \approx 10^{-3}$ for $L_{\parallel} = 2692.3$ and for visibly smaller β (around a factor $3 \div 4$) when the connection length is doubled (see Fig.2). The validity of our nonlinear estimator is therefore confirmed by these results. It is worth remarking that these results might have consequences for reactor relevant machines, which will have much longer connection lengths with respect to present day machines and could be more affected by finite β effects.

Note that we also performed scans in the perpendicular filament width, w , and we found that the onset of the electromagnetic effects had a weak dependence on this parameter. This is due to the fact that L_{\perp} is associated with the electrostatic potential rather than the density and the former changes relatively weakly with the filament's width [44, 46], so that $L_{\perp} = w$ is *not* a good approximation. Also, the situation is complicated by the fact that small filaments below the critical size [44], are already disconnected from the target, hence the role of the Alfvén waves (and hence the electromagnetic effects)

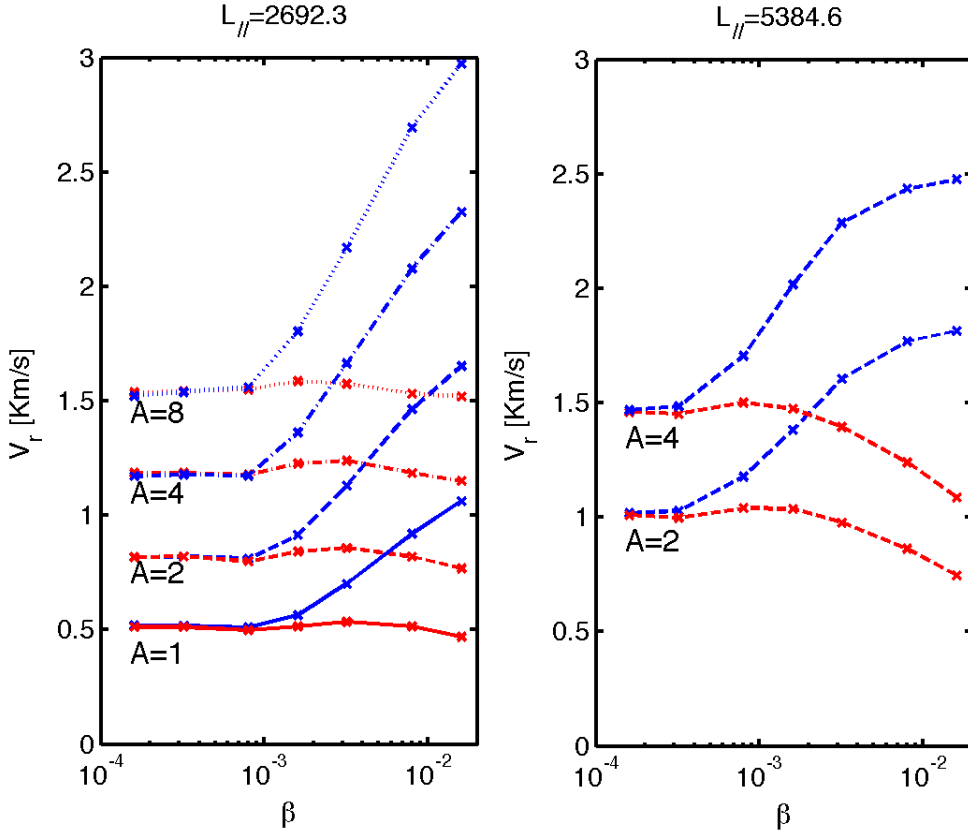


Figure 2. Scaling of the maximal radial velocity of a filament with density amplitude A and plasma β . Midplane velocity (blue) increases with plasma β , target velocity (red) decreases with plasma β (only very slightly for the smaller connection length). The left and right panel correspond to different parallel connection lengths.

becomes marginal. We conclude that the nonlinear criterion is rigorously applicable only for filaments above the critical threshold width, i.e. those that would be sheath connected if they were electrostatic.

3.2. Field Line Dynamics

Large scale behaviour in the magnetic field is present as the plasma moves into the electromagnetic regime. In particular, as β is increased, the magnetic field lines become 'frozen' into the plasma (if resistivity is small enough, as in our case), resulting in field lines being dragged by the filaments as in the well known ideal MHD picture. The freezing of the field lines, however, can be incomplete at small β and the process is always continuous and tending to complete slippage of the plasma through the magnetic field in the $\beta \rightarrow 0$ limit. This represents the transition from an almost adiabatic condition, characteristic of electrostatic dynamics, to the MHD constraint $E_{\parallel} \approx 0$ obtained by balancing the inductive and electrostatic part of the parallel electric field. Mathematically, this change of regime represents a shift in the dominant balance in Ohm's law, Eq.4, from $\nabla_{\parallel} \phi \approx \nabla_{\parallel} \log(n)$ to $(\beta/2)\partial\psi + \nabla_{\parallel} \phi \approx 0$. To investigate this, we performed simulations similar to the ones discussed in Section 3.1 but with a reduced β range and with resolution increased to $256 \times 256 \times 64$ points in order to properly capture the dynamics of the field lines.

In order to visualise field line dragging, field lines are traced from equidistant points along the target ($z = L_z$) at $y = 0$. This is performed by integrating along the magnetic field from their origin at the target. The radial position of each field line at the midplane

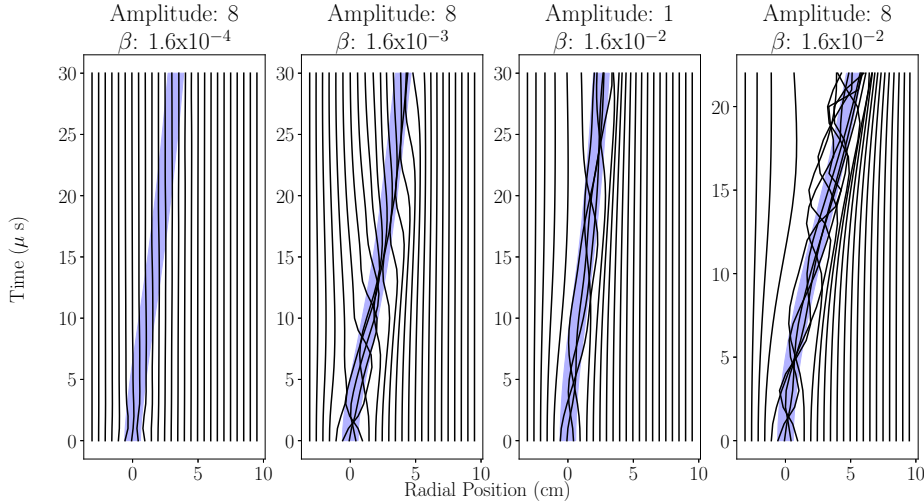


Figure 3. Magnetic field lines' radial position at the midplane over time, showing the different magnetic regimes: Electrostatic, intermediate and two electromagnetic examples. The first electromagnetic case is realistic, the second extreme for tokamaks. The blue band shows the approximate extent of the filament density perturbation.

($z = 0$) is then evolved and tracked over time to examine how it moves as a consequence of the passage of the filament. The results are shown in figure 3. In this figure the blue area gives the approximate position of the filament (i.e. the pressure perturbation), and the black lines represent the radial trajectories of field lines at the midplane - each line representing a different field line.

Three different qualitative regimes are illustrated with β values of 1.6×10^{-4} , 1.6×10^{-3} and 1.6×10^{-2} . The lowest β effectively corresponds to an electrostatic approximation, whilst the highest β is in the electromagnetic regime where the frozen in condition is well satisfied. In between these two extremes, field lines are significantly perturbed but not completely frozen into the plasma and relax within the lifetime of the filament. This excites Alfvén waves which tend to remove the field line bending produced by the passage of the filament. The final high β high amplitude case shown in Fig.3 would represent a violent perturbation like an ELM (but we do not claim here that our model can reproduce ELMs), while low amplitude, high β cases can be considered characteristic of L-mode or inter-ELM filaments produced by residual turbulence. It can be seen that at the highest β , the field lines are frozen into the small amplitude filament and there is qualitative similarity to the high β , high amplitude case.

In order to better interpret the dynamics of each field line, the midplane drift plane view is also analysed ($z = 0$). The same process is repeated with a regular grid of field lines originating at the target in order to visualise the perpendicular motions of the field lines. The trajectories of the field lines at the midplane are shown in figure 4 for two values of β . The colour represents the time at which the trajectory was in that position, contours show the filament densities of 0.2 and 2 above background at the final time instance. The same process was repeated at the target, but the results are not shown because the field lines do not have a significant excursion from their original position.

In the intermediate β case, perturbations are seen within the path the filament travelled, but the trajectories begin to return to their original positions as the field relaxes - see trajectories that almost close on themselves. In the high β case, there is a complicated movement of field lines within the filament and simpler trajectories in the surrounding region. These outer trajectories are following the $\mathbf{E} \times \mathbf{B}$ drift caused by the electrostatic

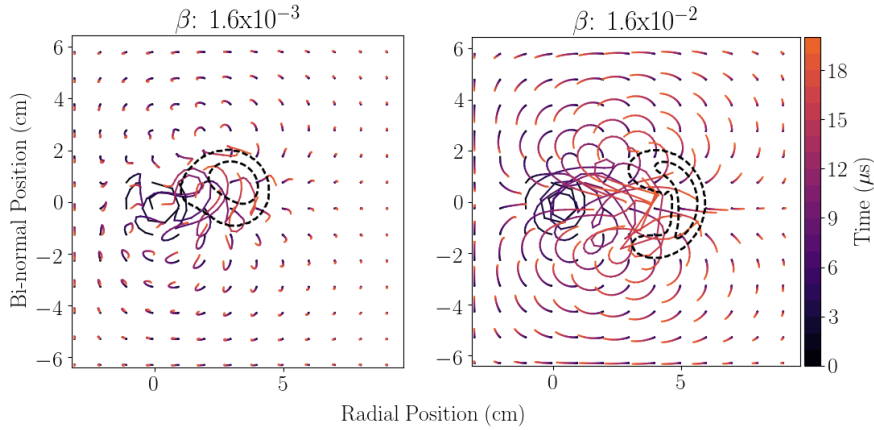


Figure 4. Trajectories of a uniform grid of field lines during the lifetime of the filament. Field lines are seeded at the target and plotted at the midplane. The filament begins at (0,0) and the density contours of 0.2 and 2 at time= $20\mu\text{s}$ are overlaid.

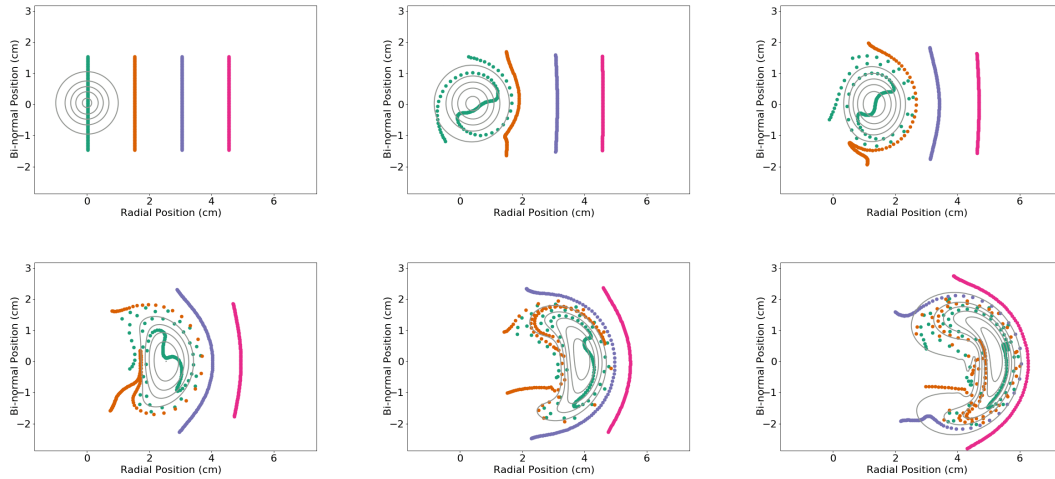


Figure 5. Midplane cross-section of filament density contours, and magnetic field lines traced from the target at $4\mu\text{s}$ intervals. Field lines get dragged along with the filament and compressed into layers at the edge of the filament.

dipole formed by the filament. The latter is the well-known cause of the filament outward radial motion [47]. Inside the filament the movement is dominated by a combination of twisting from the initial current transient due to parallel gradients and the convection cells that form within the filament structure. As the frozen in condition is partially satisfied at high β , the field line trajectories trace the movement of the fluid itself. From these visualisations it is apparent that the filament does not behave as a solid tube of plasma.

To better understand the dynamics of the magnetic field local to the filament, high resolution clusters of magnetic field lines were seeded together. Figure 5 shows such an arrangement with four arrays of closely spaced field lines traced within and in front of the initial filament location for the high β , large amplitude case. Arranged in this way, the field lines show several key dynamic behaviours. Field lines that were originally inside the filament remain inside it during its motion, showing that the frozen in condition is well satisfied. Field lines that were initially outside tend to bend around the filament as it approaches them and can be trapped within the convective cells associated with it. It is

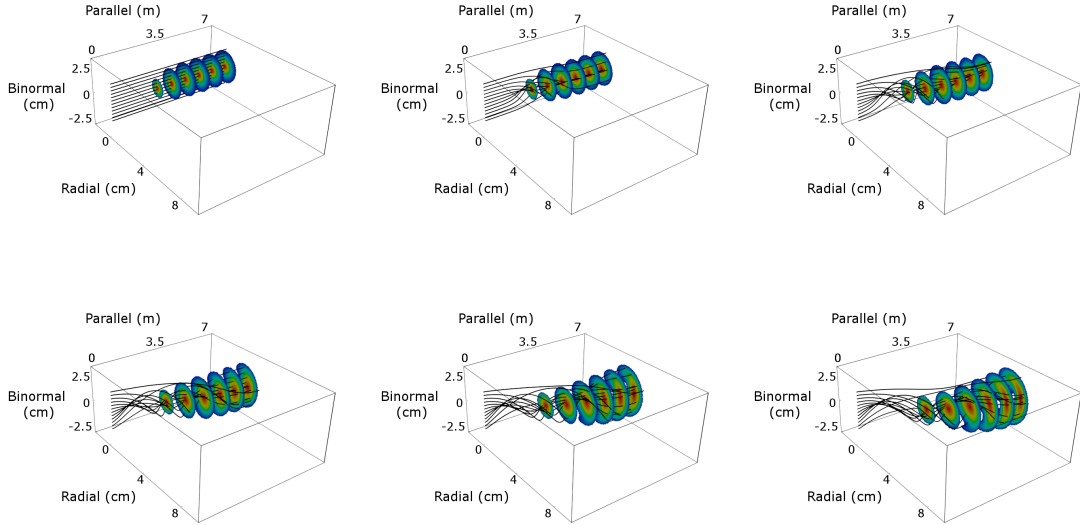


Figure 6. Field line twisting associated with the filament motion. The high β , $A = 8$ filament is represented at six different stages of its evolution (from left to right, top to bottom) as it interacts with a grid of field lines fixed at the target. Each stage of the evolution is separated by $4\mu s$. Note that only half of the domain is shown (from symmetry plane, to the right, to target, to the left).

likely that, even in this regime, some field lines will penetrate inside the filament and some will escape, but it is difficult to provide a quantitative estimate due to the fact that the filament is not a solid object and it deforms as it propagates.

Finally, we note that the parallel currents flowing in the filament in response to the diamagnetic drive [47, 24] induce perpendicular magnetic fields [37] which will tend to twist the field lines in the proximity of the pressure perturbation. This leads to a helical deformation of the field lines, which can be clearly observed in the time series shown in Fig.6.

As Figs. 3, 4, 5 and 6 show, the dynamics of the field line dragging are non-trivial, as the lines do not simply move outwards radially, with the filament centre of mass. Instead, local effects dominate their behaviour, with the field lines being twisted around. Clusters of straight field lines initially lying on the same plane become 3D loops around the filament. The planes that begin within the filament make several loops around it while those further in front wrap around it but the ends trail behind. As Fig. 3 shows, the field lines somewhat in front of the filament are pushed radially forwards as the filament moves, but at a slower velocity than the filament. The field lines gather towards the edge of the filament and become dense, showing field line compression, a possible sign that current sheets will develop in the filament. This poses the question of whether magnetic reconnection could occur in these current sheets, an interesting subject that we leave for future investigation [49]. The filament then meets the compressed field lines and draws them around the density perturbation (see Figs.4 and 5). Field lines that begin separated by several filament widths end within a thin layer at the edge of the filament.

4. Discussion and Conclusions

It has been shown that electromagnetic effects arising from finite β can affect the dynamics of Scrape Off Layer filaments, which then perturb the magnetic field as they pass through. Under the parameter range investigated, which is relevant for MAST plasmas in the

proximity of the separatrix [53], but is easily generalizable, these effects become apparent at β as low as 1×10^{-3} , e.g. for typical H-mode conditions in a medium size tokamak with $n_{sep} \sim 2 \times 10^{19} m^{-3}$, $T_{sep} \sim 100 eV$ and $B \sim 1T$. The electrostatic approximation is probably sensible for the far SOL where the plasma β is smaller, but the electromagnetic effects should be included as simulations are performed in hotter and denser regions. It is important to remark that small filaments below the critical size [44] are already disconnected and therefore the results of this paper are less relevant for them. Filaments around the critical size (such as those studied in our investigation where $w = 5 \sim w_{cr}$) will be affected but larger filaments well above the critical size are the ones where the disconnection produces the more striking changes in propagation velocity.

A nonlinear criterion to estimate when electromagnetic effects become important for sheath connected filaments was introduced and it resembles similar criteria for edge turbulence [51, 52, 41]. Broadly speaking, three regimes of behaviour were identified: the two limits of electrostatic [$\beta \ll (L_{\perp} c_s)^2 / (L_{\parallel} V_{\perp})^2$] and electromagnetic regimes [$\beta \gg (L_{\perp} c_s)^2 / (L_{\parallel} V_{\perp})^2$], with a third regime between the two. When taking $L_{\perp} \sim 1cm$ and $V_{\perp} \sim 0.01c_s$ as the filament width and typical perpendicular velocity, the characteristic β is relatively small. This criterion can be easily shown to be a generalisation of the one presented in [37], which implicitly assumes that $V_{\perp} = L_{\perp} \gamma_{MHD} \sim c_s \sqrt{L_{\perp} / R}$ and therefore specialises for ballooning mode perturbations which are *not* connected to the sheath to begin with [48].

As our simulations showed, we therefore expect realistic filaments to show non-negligible electromagnetic effects, including bending of the perturbation in the parallel direction, dragging of the field lines and effective electrical disconnection from the target (and consequent faster cross field velocity). Importantly, these effects are significant only for filaments that would be, at least partially, electrically connected with the sheath if they were at low β . Filaments with small cross section in the inertial range, where the polarisation current dominates over the sheath effects, are much less sensitive to the electromagnetic effects discussed here as they already lack communication with the target.

Bending of plasma filaments in electromagnetic regimes has been shown qualitatively in previous work by Lee *et al* [39, 40]. Our investigation can be seen as a natural extension of that work, with the additional quantification of changes in the radial velocities at the midplane and target. With increasing β , the radial velocity of plasma filaments increases at the midplane (up to 100% in the simulations reported here), and decreases at the target. This has been interpreted using Alfvén waves which travel more slowly (relative to the sound speed, i.e the filament's characteristic velocity) at higher plasma β and communicate information about the electromagnetic field along the filament. If they are slow enough the midplane segment of filament generates strong electric fields without being affected by the target, which cannot be mitigated by the sheath impedance and sink effect of the target. With this interpretation, geometric modifications in the tokamak such as the length of the divertor leg could lead to enhanced electromagnetic effects in the filament. With a sufficiently long connection length, the central section of the filament will behave as if it is not attached to any target.

We also described how the filaments affect the magnetic field by dragging and braiding the magnetic field lines with the movement of the fluid elements within the filament. The complex motion of the field lines results from them being increasingly frozen into the plasma at high β and so displaced by the dipolar convection cells formed in the filaments. In addition, parallel currents act to twist the magnetic field lines into helices. At high β , field lines within the filament do not leave, but the leading edge of the filament does draw in new field lines it encounters. Parallel communication becomes delayed and different sections of the filament behave differently. The internal fluid motions of the filament also play a strong role in the field line dynamics.

As a result of the coupling between fluid motion and magnetic field lines, the filament

can leave a magnetic wake, which might affect the motion of following filaments. Further work is required to examine the long term behaviour of the filaments in these conditions and the overall effect on perpendicular transport. Future work will also look into magnetic reconnection and the role of currents in the filament [49]. Long term goals include more realistic magnetic geometry and to study how the filament interacts with the separatrix as it moves from the core to the SOL, as these, at the moment, are the biggest limitations of the work presented here.

Acknowledgements

We thank Dr. D. Moulton for carefully reading the manuscript. This work was funded by the RCUK Energy Programme [grant number EP/P012450/1]. The simulations presented herein were carried out in part on the CINECA Marconi supercomputer within the framework of the SOL_BOUT project and in part using Archer computing resources under Plasma HEC consortium grants EP/L000237/1 and EP/R029148/1. This work was in part supported by the UK EPSRC funded Collaborative Computational Project in Plasma Physics - grant reference number EP/M022463/1. To obtain further information on the data and models underlying this paper, whose release may be subject to commercial restrictions, please contact PublicationsManager@ukaea.uk.

References

- [1] D.A. D'Ippolito, J.R. Myra and S.J. Zweben, *Phys. Plasmas* 18, 060501 (2011).
- [2] A. Kirk, N. Ben Ayed, G. Counsell, B. Dudson, T. Eich, A. Herrmann, B. Koch, R. Martin, A. Meakins, S. Saarelma, R. Scannell, S. Tallents, M. Walsh and H.R. Wilson, *Plasma Phys. Control. Fusion* 48, B433 (2006).
- [3] B.D. Dudson, N. Ben Ayed, A. Kirk, H.R. Wilson, G. Counsell, X. Xu, M. Umansky, P.B. Snyder and B. Lloyd, *Plasma Phys. Control. Fusion* 50, 124012 (2008).
- [4] N. Ben Ayed, A. Kirk, B. Dudson, S. Tallents, R.G.L. Vann and H.R. Wilson, *Plasma Phys. Control. Fusion* 51, 035016 (2009).
- [5] F. Militello, N.R. Walkden, T. Farley, W.A. Gracias, J. Olsen, F. Riva, L. Easy, N. Fedorczak, I. Lupelli, J. Madsen, A.H. Nielsen, P. Ricci, P. Tamain and J. Young, *Plasma Phys. Control. Fusion* 58, 105002 (2016).
- [6] B. LaBombard, R. L. Boivin, M. Greenwald, J. Hughes, B. Lipschultz, D. Mossessian, C. S. Pitcher, J. L. Terry, S. J. Zweben, *Phys. Plasmas* 8, 2107 (2001).
- [7] J. A. Boedo, D. Rudakov, R. Moyer, S. Krasheninnikov, D. Whyte et al., *Phys. Plasmas* 8, 4826 (2001).
- [8] D.L. Rudakov, J.A. Boedo, R.A. Moyer, S. Krasheninnikov, A.W. Leonard, M.A. Mahdavi, G.R. McKee, G.D. Porter, P.C. Stangeby, J.G. Watkins, W.P. West, D.G. Whyte and G. Antar, *Plasma Phys. Control. Fusion* 44, 717 (2002).
- [9] J. A. Boedo, D. L. Rudakov, R. A. Moyer, G. R. McKee, R. J. Colchin, M. J. Schaffer, P. G. Stangeby, W. P. West, S. L. Allen, T. E. Evans, R. J. Fonck, E. M. Hollmann, S. Krasheninnikov, A. W. Leonard, W. Nevins, M. A. Mahdavi, G. D. Porter, G. R. Tynan, D. G. Whyte, and X. Xu, *Phys. Plasmas* 10, 1670 (2003).
- [10] O.E. Garcia, J. Horacek, R.A. Pitts, A.H. Nielsen, W. Fundamenski, V. Naulin and J. Juul Rasmussen, *Nucl. Fusion* 47, 667 (2007).
- [11] O.E. Garcia, R.A. Pitts, J. Horacek, J. Madsen, V. Naulin, A.H. Nielsen and J.J Rasmussen, *Plasma Phys. Control. Fusion* 49, B47 (2007).
- [12] F. Militello, P. Tamain, W. Fundamenski, A. Kirk, V. Naulin and A.H. Nielsen, *Plasma Phys. Control. Fusion* 55, 025005 (2013).
- [13] S. J. Zweben, D. P. Stotler, J. L. Terry, B. LaBombard, M. Greenwald, M. Muterspaugh, C. S. Pitcher, Alcator CMod Group, K. Hallatschek, R. J. Maqueda, B. Rogers, J. L. Lowrance, V. J. Mastrocola, and G. F. Renda, *Phys. Plasmas* 9, 1981 (2002).
- [14] J. L. Terry, S. J. Zweben, K. Hallatschek, B. LaBombard, R. J. Maqueda, B. Bai, C. J. Boswell, M. Greenwald, D. Kopon, W. M. Nevins, C. S. Pitcher, B. N. Rogers, D. P. Stotler, and X. Q. Xu, *Phys. Plasmas* 10, 1739 (2003).

- [15] J. R. Myra, D. A. D'Ippolito, D. P. Stotler, S. J. Zweben, B. P. LeBlanc, J. E. Menard, R. J. Maqueda and J. Boedo, *Physics of Plasmas* 13, 092509 (2006).
- [16] O. E. Garcia, S. M. Fritzner, R. Kube, I. Cziegler, B. LaBombard, and J. L. Terry, *Physics of Plasmas* 20, 055901 (2013).
- [17] S. J. Zweben, J.R. Myra, W.M. Davis, D.A. D'Ippolito, T.K. Gray, S.M. Kaye, B.P. LeBlanc, R.J. Maqueda, D.A. Russell and D.P. Stotler, *Plasma Phys. and Control. Fusion* 58, 044007 (2016).
- [18] O.E. Garcia, V. Naulin, A.H. Nielsen and J.J. Rasmussen, *Phys. Rev. Lett.* 92, 165003 (2004).
- [19] F. Militello, V. Naulin and A.H. Nielsen, *Plasma Phys. Control. Fusion* 55, 074010 (2013).
- [20] F. Riva, C. Colin, J. Denis, L. Easy, I. Furno, J. Madsen, F. Militello, V. Naulin, A.H. Nielsen, J.M.B. Olsen, J.T. Omotani, J.J. Rasmussen, P. Ricci, E. Serre, P. Tamain and C. Theiler, *Plasma Phys. Control. Fusion* 58, 044005 (2016).
- [21] L. Easy, F. Militello, J. Omotani, B. Dudson, E. Havlíčková, P. Tamain, V. Naulin, and A. H. Nielsen, *Phys. Plasmas* 21, 122515 (2014).
- [22] L. Easy, F. Militello, J. Omotani, B. Dudson, *Physics of Plasmas* 23, 012512 (2016).
- [23] N.R. Walkden, L. Easy, F. Militello and J.T. Omotani, *Plasma Phys. Control. Fusion* 58, 115010 (2016) .
- [24] J. Omotani, F. Militello, L. Easy and N.R. Walkden, *Plasma Phys. Control. Fusion* 58, 014030 (2015).
- [25] W. Fundamenski, O.E. Garcia, V. Naulin, R.A. Pitts, A.H. Nielsen, J.J. Rasmussen, J. Horacek, J.P. Graves, *Nucl. Fusion* 47, 417 (2007).
- [26] B.D. Dudson, A. Allen, G. Breyiannis, E. Brugger, J. Buchanan, L. Easy, S. Farley, I. Joseph, M. Kim, A.D. McGann, J.T. Omotani, M.V. Umansky, N.R. Walkden, T. Xia and X. Q. Xu, *Journal of Plasma Physics*, 81(1), 365810104 (2015).
- [27] P. Ricci, F.D. Halpern, S. Jolliet, J. Loizu, A. Masetto, A. Fasoli, I. Furno and C. Theiler, *Plasma Phys. Control. Fusion* 54, 124047 (2012).
- [28] F.D. Halpern, P.Ricci, S.Jolliet, J.Loizu, J.Morales, A.Mosetto, F.Musil, F.Riva, T.M.Tran, C.Wersal, *J. Comput. Phys.* 315, 388–408 (2016).
- [29] A.H. Nielsen, G. Xu, J. Madsen, V. Naulin, J.J. Rasmussen and B. Wan, *Phys. Lett. A.* 379, 3097 (2015).
- [30] J. Madsen, V. Naulin, A.H. Nielsen, and J.J. Rasmussen, *Phys. Plasmas* 23, 032306 (2016).
- [31] P. Tamain, H. Bufferand, G. Ciraolo, C. Colin, P. Ghendrih, F. Schwander and E. Serre, *Contrib. Plasma. Phys.* 54, 555 (2014).
- [32] S. Krasheninnikov, D.D. Ryutov and G. Yu, *J. Plasma Fusion Res. Series* 6, 139 (2004).
- [33] T.T. Ribeiro and B. Scott, *Plasma Phys. Control. Fusion* 47, 1657–1679 (2005).
- [34] J.R. Myra and D.A. D'Ippolito, *Phys. of Plasmas* 12, 092511 (2005).
- [35] G.Q. Yu, S.I. Krasheninnikov, and P.N. Guzdar, *Phys. Plasmas* 13, 042508 (2006).
- [36] T.T. Ribeiro and B. Scott, *Plasma Phys. Control. Fusion* 50, 055007 (2008).
- [37] S.I. Krasheninnikov, D. Ryutov, G.Q. Yu, *J. Plasma Fusion Res. SERIES* 6, 139 (2004).
- [38] G.S. Xu, V. Naulin, W. Fundamenski, C. Hidalgo, J.A. Alonso, C. Silva, B. Goncalves, A.H. Nielsen, J.J. Rasmussen, S.I. Krasheninnikov, B.N. Wan, M. Stamp and JET EFDA Contributors, *Nucl. Fusion* 49, 092002 (2009).
- [39] W. Lee, M.V. Umansky, J.R. Angus, and S.I. Krasheninnikov, *Physics of Plasmas* 22, 012505 (2015).
- [40] W. Lee, M.V. Umansky, J.R. Angus, and S.I. Krasheninnikov, *J. Nucl. Mat.* 463, 765 (2015).
- [41] B. Scott, *Plasma Phys. Control. Fusion* 39, 1635 (1997).
- [42] F. Militello, B. Dudson , L. Easy, A. Kirk and P. Naylor, *Plasma Phys. Control. Fusion* 59, 125013 (2017).
- [43] L. Easy, "Three Dimensional Simulations of Scrape-Off Layer Filaments", PhD thesis, York University (2016).
- [44] G. Q. Yu and S. I. Krasheninnikov, *Physics of Plasmas* 10, 4413 (2003).
- [45] D. A. D'Ippolito, J. R. Myra and D. A. Russell, S. I. Krasheninnikov, A. Yu. Pigarov and G. Q. Yu, X. Q. Xu and W. M. Nevins, 20th IAEA Fusion Energy Conference, Vilamoura, Portugal, Nov. 1-6, (2004)
- [46] N.R. Walkden, B.D. Dudson and G. Fishpool, *Plasma Phys. Control. Fusion* 55, 105005 (2013).
- [47] S.I. Krasheninnikov, *Phys. Lett. A* 283, 368 (2001).
- [48] J. R. Myra, D. A. Russell, and D. A. D'Ippolito, *Phys. Plasmas* 13, 112502 (2006).
- [49] F. Militello *et al.*, EM in preparation

- [50] A.N. Simakov and P.J. Catto, *Phys. Plasmas* 10, 4744 (2003).
- [51] A.B. Mikhailovskii and L.I. Rudakov *Sov. Phys-JETP* 17, 621 (1963).
- [52] J.T. Tang and N.C. Jr Luhmann *Phys. Fluids* 19, 1935 (1976).
- [53] F. Militello and W. Fundamenski, *Plasma Phys. Control. Fusion* 53, 095002 (2011).